AWARD NUMBER: W81XWH-13-1-0244

TITLE:
Identification, Characterization, and Utilization of Adult Meniscal Progenitor Cells

PRINCIPAL INVESTIGATOR: Dr. Vicki Rosen

CONTRACTING ORGANIZATION: Harvard College, President and Fellows of
Boston, MA 02115

REPORT DATE: September 2015

TYPE OF REPORT: Annual

PREPARED FOR: U.S. Army Medical Research and Materiel Command
Fort Detrick, Maryland 21702-5012

DISTRIBUTION STATEMENT: Approved for Public Release;
Distribution Unlimited

REPORT DOCUMENTATION PAGE

Form Approved
OMB No. 0704-0188

1. REPORT DATE	**2. REPORT TYPE**	**3. DATES COVERED**
September 2015	Annual	1 Sep 2014 - 31 Aug 2015

4. TITLE AND SUBTITLE
Identification, Characterization, and Utilization of Adult Meniscal Progenitor Cells

5a. CONTRACT NUMBER

5b. GRANT NUMBER
W81XWH-13-1-0244

5c. PROGRAM ELEMENT NUMBER

6. AUTHOR(S)
Vicki Rosen

E-Mail:Vicki_Rosen@hsdm.harvard.edu

5d. PROJECT NUMBER

5e. TASK NUMBER

5f. WORK UNIT NUMBER

7. PERFORMING ORGANIZATION NAME(S) AND ADDRESS(ES)
AND ADDRESS(ES)
Harvard School of Dental Medicine
188 Longwood Ave., REB 510
Boston, MA 02115-6027

8. PERFORMING ORGANIZATION REPORT NUMBER

9. SPONSORING / MONITORING AGENCY NAME(S) AND ADDRESS(ES)

U.S. Army Medical Research and Materiel Command
Fort Detrick, Maryland 21702-5012

10. SPONSOR/MONITOR'S ACRONYM(S)

11. SPONSOR/MONITOR'S REPORT NUMBER(S)

12. DISTRIBUTION / AVAILABILITY STATEMENT

Approved for Public Release; Distribution Unlimited

13. SUPPLEMENTARY NOTES

14. ABSTRACT

Meniscal injuries are the most common traumatic leg injuries, accounting for over half of the knee arthroscopies performed each year. Damaged menisci rarely regain normal structural integrity or mechanical strength, and surgical repair cannot reliably prevent the degenerative changes that occur post injury and presage the development of knee osteoarthritis (OA). New treatments centered on the stem/progenitor cell population resident within the adult meniscus will be key to derailing the connection between acute meniscal injury and post-traumatic knee OA. Here we combine mouse genetics with molecular and cell biology to develop a profile of repair cells in the adult meniscus, track meniscal stem/progenitor cell (MSPC) behavior within meniscus as function of age, and assess the contribution of resident MSPCs to repair after meniscal injury. During the current research period we made significant progress toward our goals by establishing a standard protocol for harvesting MSPCs from 8 week, 6 month and 1-year old mouse menisci. MSPCs grow as colonies, express stem cell and meniscal gene signature markers found in adult human meniscus, and can be successfully passaged. We also piloted a novel mouse meniscal tear injury model, and are now ready to use this technique for experiments outlined in our proposal.

15. SUBJECT TERMS
meniscus, meniscal cells, stem cells, progenitor cells, meniscus healing, meniscus repair, osteoarthritis

16. SECURITY CLASSIFICATION OF:			**17. LIMITATION OF ABSTRACT**	**18. NUMBER OF PAGES**	**19a. NAME OF RESPONSIBLE PERSON**
a. REPORT	**b. ABSTRACT**	**c. THIS PAGE**			USAMRMC
Unclassified	Unclassified	Unclassified	Unclassified	19	**19b. TELEPHONE NUMBER** *(include area code)*

Table of Contents

Page

1. Introduction……...4

2. Keywords……...4

3. Overall Project Summary……....4

4. Key Research Accomplishments…….9

5. Conclusion…….9

6. Publications, Abstracts, and Presentations……..…..……...9

7. Inventions, Patents and Licenses…….....9

8. Reportable Outcomes..……10

9. Other Achievements……10

10. References……...10

11. Appendices……..10

1. Introduction

Meniscal injuries are the most common of traumatic knee injuries. Once damaged, meniscal tissue rarely regains normal structural integrity and mechanical strength. Surgical repair of meniscal tears cannot reliably prevent the degenerative changes that occur after injury. As a result, meniscal injuries are a common underlying cause of post-traumatic osteoarthritis. This is particularly striking in young, healthy individuals such as military personnel, where meniscal injury is often associated with long-term disability and knee replacement surgery. This proposal focuses on identifying meniscal stem/progenitor cells (MSPC) in the adult meniscus, developing a molecular profile of these cells, and examining the contribution MSPC provide to repair after meniscal injury. Information gathered from these studies will be useful for developing new treatments for acute meniscal injuries, lessening the need for joint replacement and reducing long-term disability in active adults.

2. Keywords

meniscus, meniscal cells, stem cells, progenitor cells, meniscus healing, meniscus repair, osteoarthritis

3. Overall Project Summary

Specific Aim 1.

Task 3: Characterize meniscal cells

Subtask (3a) Stem cell-like cell characteristics of MSPCs will be assessed using flow cytometry using the following markers: Sca1, CD45, CD31, CD34 CD90.2, Flk-1, CD44, and CD146. All flow cytometry analysis was performed at the Harvard Stem Cell Core facility.

For flow cytometry analysis, the mouse meniscus explant culture protocol detailed in our previous progress report was used. From a single 8 wk old mouse, 1.275-2.7 $x10^5$ meniscus cells (P0) were obtained after 15-20 days in culture. These cells were passaged into a new 10cm dish and grown to 90-100% confluence. This yielded enough P1 cells (1-2 x 10^6) cells for flow cytometry analysis. For each stem cell marker, we used 0.5 x 10^6 cells and ran two flow cytometry samples per animal. For staining, each sample was resuspended in 100µl of flow cytometry buffer and kept on ice to preserve viability and prevent antibody capping. The Fc-Block was added to each tube at the recommended concentration for cell number/density and incubated for 5 mins. The stem cell marker antibody was then added at different dilutions and incubated on ice for 30 min. These cells were washed 3 times, resuspended in 400µl of flow cytometry buffer and the samples were kept on ice protected from light until analysis. Using a series of stem cell marker antibody concentrations, the saturation point was found for each marker (Sca1 – 2µg/ml; CD45 5µg/ml; CD90.2 2.5 µg/ml; CD44 5 µg/ml) and this was used in subsequent experiments. The

MSPCs were 97.3 % positive for the mesenchymal stromal cell marker CD44, 87.8% positive for the stem cell marker, stem cell antigen-1 (Sca1), and 54% positive for CD90.2, a surface marker for fibroblasts. Only 2.3% of these cells expressed CD45, a leukocyte/hematopoietic cell marker. This flow cytometry profile was similar to what was seen for human MSPCs cultured and analyzed in a similar manner and suggests these cells have characteristics of mesenchymal stem cells.

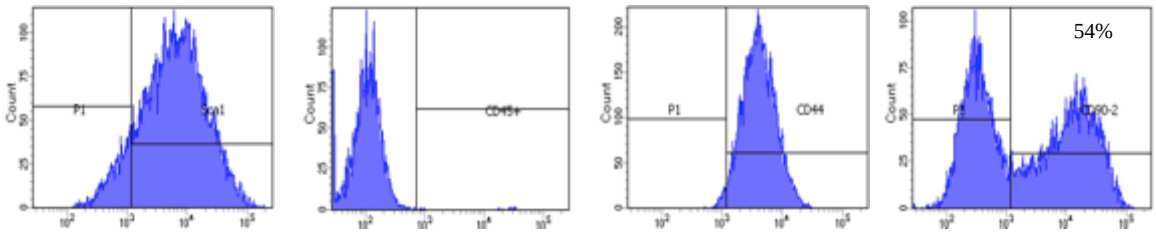

Figure 1. Flow cytometry analysis of expression of cell surface markers related to stem cells.

Subtask (3b) Clonogenicity of the population will be determined by examining the ability of single cells to form colonies. Colonies will be compared for frequency and size.

For colony forming assays, meniscus cells (P1) from 8wk old mice were seeded a density of 1000/25cm^2 flask and 2000/25cm^2 flask. MSPCs were cultured in regular growth medium for 12 days and stained with methyl violet (0.5%). Only colonies containing more than 50 cells were counted. A small population (2-3%) of meniscus derived cells formed adherent colonies similar to what was reported for tendon progenitor stem cells. These colonies were varied in size and morphology reflecting the inherent heterogeneous nature of meniscal tissue.

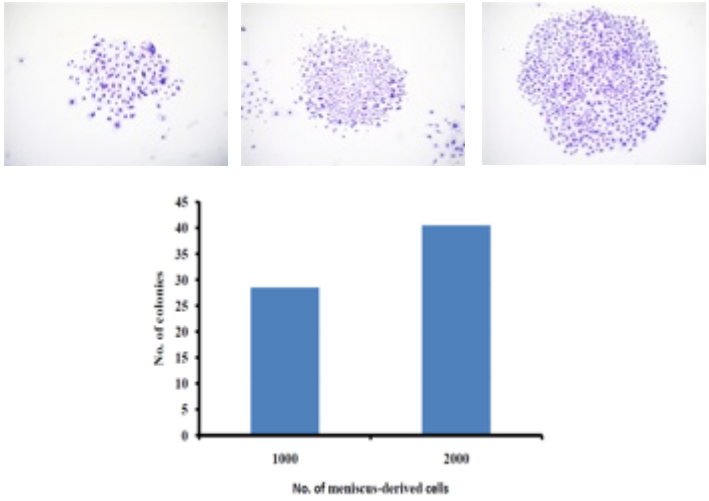

Figure 2. The colony forming efficiency of MSPCs.

Subtask (3d) Multipotentiality of the MSPCs will be evaluated by placing single cells in adipogenic, osteogenic, and chondrogenic media for 21 days, and then staining colonies with oil red O (adipogenesis), Alcian blue (chondrogenesis) and alkaline phosphatase (osteogenesis).

To evaluate the multipotentiality of MSPCs, 2 methods were tested using menisci from 8wk old mice knees. First, MSPCs were seeded at colony forming densities (1000/25cm^2 flask and 2000/25cm^2 flask) and the growth medium was changed to differentiation media (adipogenic, osteogenic, or chondrogenic) on the second day. The cells were then cultured for 12 days and stained with oil red O (adipogenesis), Alcian blue (chondrogenesis) and alkaline phosphatase (osteogenesis). Using this protocol, only a few colonies stained positive for oil red O and did not stain for the other lineages. For the second method, MSPCs were seeded at colony forming densities (1000/25cm^2 flask and 2000/25cm^2 flask) and cultured in regular growth medium for 12 days until colonies formed. Then, the growth medium was changed to differentiation media and the cells were cultured for another 7 days and stained for adipogenesis, chondrogenesis, osteogenesis. Using this protocol, colonies were able to differentiate into fat, cartilage and bone suggesting that the MSPCs are multipotential.

Subtask (3e) RNA will be collected from parallel cultures for measurement of meniscus signature genes, stem cell markers as well as markers that identify bone, cartilage, tendon and fat using Nanostring technology.

RNA was isolated from MSPCs (P1) grown to confluence for 7 days in control media from 8wk, 24wk and 52wk old mouse meniscal explants. Real time PCR was used to analyze gene expression for cells from all time points.

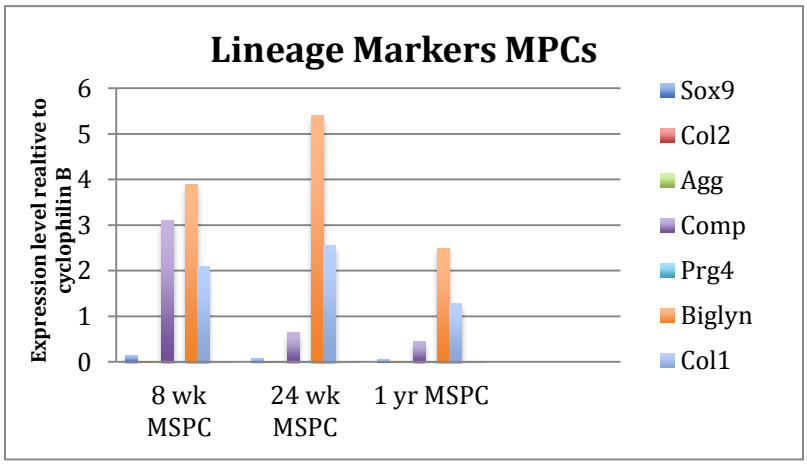

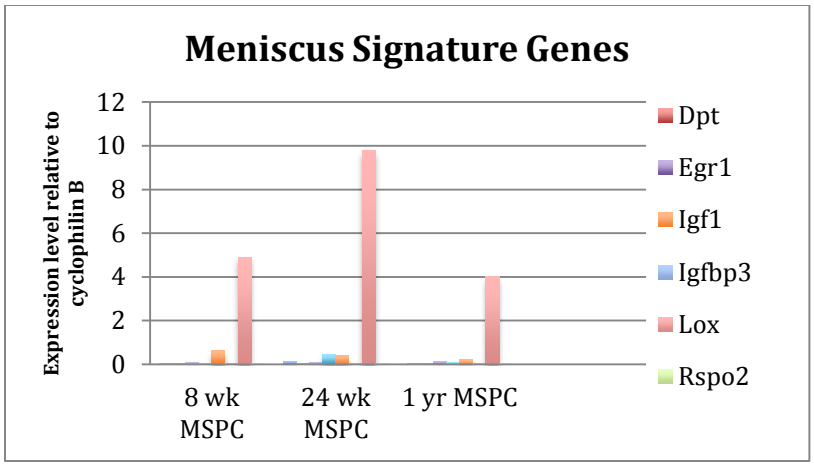

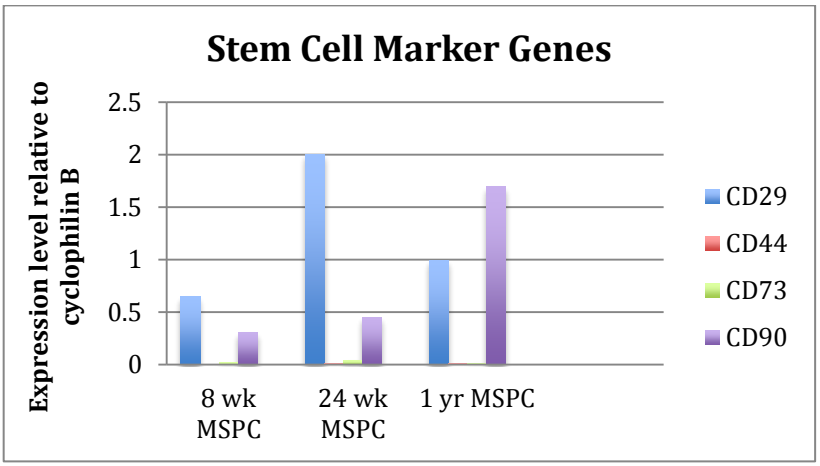

Figure 3. Real time PCR analysis of gene expression in MSPCs from 8wk, 24wk and 52wk mice meniscal explants.

qPCR analysis revealed that MSPCs from mice of all ages were positive for the mesenchymal stem cell markers CD29 and CD90/Thy1 with a peak of CD29 at 24wk and CD90 at 52wks. The MSPCs expressed robust levels of the meniscus signature gene Lox, an enzyme responsible for collagen cross-links in the musculoskeletal system. In addition, cells from young and aged mice expressed relatively steady levels of biglycan and Collagen type I, but COMP (Cartilage Oligomeric Matrix Protein) levels appeared to decrease at 6 months. This pattern of gene expression in MSPCs of all ages shows a mixed population of cells that reflects the fibro-cartilaginous composition of the adult meniscus. Our data suggest that there is not a significant difference in the gene expression profiles of MSPCs from 8wk, 24wk and 52wk old mice.

Specific Aim2.

Task 5: Assess functional changes in meniscus due to addition of MSPC.

Functional changes in meniscus due to addition of MSPC will be measured using AFM-N at the 8 wk time point. For each sample, nanoindentation will be performed in different circumferential locations at 0.316-10um/s AFM z-piezo displacement rates and total indentation depth up to ~200nm (1.5uN force).

Using a mouse model already established in our lab that has defects in meniscal maturation (BMP2-Gdf5 cKO), we evaluated the capacity of AFM-N (Atomic Force Microscopy with Nanoindentation) to reproducibly identify changes in the meniscus from 8-10wk old mice. AFM-N was able to detect significant changes in menisci from control and trangenic mice and will be a valuable tool for assessing the biomechanical changes in the menisci due to the addition of MSPCs in wild type and injured mice knees.

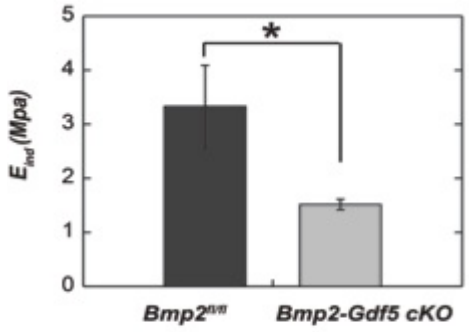

Average E_{ind} of all tested 10 week Bmp2$^{fl/fl}$ (n=6) and *Bmp2-Gdf5 cKO* (n=6) meniscus samples at 10 μm/s indentation rate shows significant difference. (*: $p = 0.0388$, $p < 0.05$, *two sample t-test)*

Figure 4. Analysis of biomechanical properties of menisci using AFM-N.
Menisci from BMP2-Gdf5 conditional knock out mice are weaker with a significantly reduced effective indentation modulus when compared to controls.

Specific Aim 3.

Task 3: Production of meniscus tear.

One week after injection of genetically labeled primary meniscal cells, a surgical tear will be made in the anterior horn of the medial meniscus using an open knee protocol.

We performed pilot studies on knee joints from mice sacrificed for other experiments to practice the meniscus injury model. For surgical tear of medial meniscus, the joint capsule immediately medial to the patellar tendon was incised and opened with a #15 blade. Without cutting the ligaments, the medial meniscus was identified. Using a 30G needle, trephination of the front of the meniscal body was

performed to make a small surgical tear. Once the injury of the meniscus was made, the knees were fixed and processed for histological analysis.

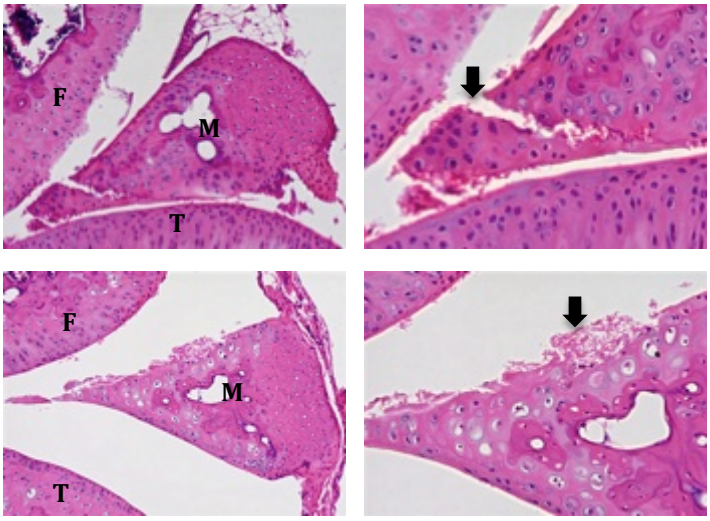

Figure 5. Histological analysis of surgical tears of medial meniscus. Sections of meniscus were stained with Hematoxylin and Eosin. Arrows indicate tear. F=Femur; T=Tibia; M=Meniscus.

Using a 30G needle we were able to make a small, discrete injury to the inner portion of the medial meniscus. With continued practice, we are confident we can reproducibly make this tear and use this as our meniscus injury model for injection of MSPCs.

4. Key Research Accomplishments

Nothing to Report.

5. Conclusion

Nothing to Report.

6. Publications, Abstracts, and Presentations

Li Q, Doyran B, Gamer L, Lu X, Qin L, Ortiz C, Grodzinsky A, **Rosen V**, Han L. Biomechanical properties of murine meniscus surface via AFM-based nanoindentation. *J Biomech.* 2015; 48:1364-1370; PMID: 25817332.

7. Inventions, Patents and Licenses

Nothing to Report.

8. Reportable Outcomes

Nothing to Report.

9. Other Achievements

This funding has resulted in post-doctoral training of Rui Rui Shi, MD, PhD.

10. References

None.

11. Appendices

a. Li Q, Doyran B, Gamer L, Lu X, Qin L, Ortiz C, Grodzinsky A, **Rosen V**, Han L. Biomechanical properties of murine meniscus surface via AFM-based nanoindentation. *J Biomech.* 2015; 48:1364-1370; PMID: 25817332.

b. CV of Rui Rui Shi

Journal of Biomechanics 48 (2015) 1364–1370

Contents lists available at ScienceDirect

Journal of Biomechanics

journal homepage: www.elsevier.com/locate/jbiomech
www.JBiomech.com

Biomechanical properties of murine meniscus surface via AFM-based nanoindentation

Qing Li [a], Basak Doyran [a], Laura W. Gamer [b], X. Lucas Lu [c], Ling Qin [d], Christine Ortiz [e], Alan J. Grodzinsky [f,g,h], Vicki Rosen [b], Lin Han [a,*]

[a] School of Biomedical Engineering, Science, and Health Systems, Drexel University, Philadelphia, PA 19104, United States
[b] Department of Developmental Biology, Harvard School of Dental Medicine, Boston, MA 02115, United States
[c] Department of Mechanical Engineering, University of Delaware, Newark, DE 19716, United States
[d] Department of Orthopaedic Surgery, University of Pennsylvania, Philadelphia, PA 19104, United States
[e] Department of Materials Science and Engineering, Massachusetts Institute of Technology, Cambridge, MA 02139, United States
[f] Department of Biological Engineering, Massachusetts Institute of Technology, Cambridge, MA 02139, United States
[g] Department of Electrical Engineering and Computer Science, Massachusetts Institute of Technology, Cambridge, MA 02139, United States
[h] Department of Mechanical Engineering Massachusetts Institute of Technology, Cambridge, MA 02139, United States

ARTICLE INFO

Article history:
Accepted 28 February 2015

Keywords:
Meniscus
Mouse models
Atomic force microscopy
Nanoindentation
Anisotropy

ABSTRACT

This study aimed to quantify the biomechanical properties of murine meniscus surface. Atomic force microscopy (AFM)-based nanoindentation was performed on the central region, proximal side of menisci from 6- to 24-week old male C57BL/6 mice using microspherical tips ($R_{tip} \approx 5$ μm) in PBS. A unique, linear correlation between indentation depth, D, and response force, F, was found on menisci from all age groups. This non-Hertzian behavior is likely due to the dominance of tensile resistance by the collagen fibril bundles on meniscus surface that are mostly aligned along the circumferential direction. The indentation resistance was calculated as both the effective modulus, E_{ind}, via the isotropic Hertz model, and the effective stiffness, $S_{ind} = dF/dD$. Values of S_{ind} and E_{ind} were found to depend on indentation rate, suggesting the existence of poro-viscoelasticity. These values do not significantly vary with anatomical sites, lateral versus medial compartments, or mouse age. In addition, E_{ind} of meniscus surface (e.g., 6.1 ± 0.8 MPa for 12 weeks of age, mean ± SEM, $n=13$) was found to be significantly higher than those of meniscus surfaces in other species, and of murine articular cartilage surface (1.4 ± 0.1 MPa, $n=6$). In summary, these results provided the first direct mechanical knowledge of murine knee meniscus tissues. We expect this understanding to serve as a mechanics-based benchmark for further probing the developmental biology and osteoarthritis symptoms of meniscus in various murine models.

1. Introduction

Knee meniscus is a hydrated fibrocartilage tissue with an extracellular matrix (ECM) mainly composed of circumferentially aligned, type I-dominated collagen fibers (≈ 20–25 wet wt%) and small amounts of proteoglycans (< 5 wet wt%) (Aspden et al., 1985; Herwig et al., 1984). In human menisci, the circumferential fibers are wrapped within the superficial layer made of radially aligned fibers, which is covered by a thin mesh of transversely aligned fibrils on the surface (Petersen and Tillmann, 1998). Within the interior of the meniscus, circumferential fibers are further interdigitated by "radial-tie" fibers throughout (Skaggs et al., 1994). This hierarchically structured, heterogeneous ECM provides meniscus with its biomechanical functions paramount to joint motion, including load distribution (Walker and Erkman, 1975), shock absorption (Voloshin and Wosk, 1983) and lubrication (Fithian et al., 1990). During the progression of osteoarthritis (OA), meniscus often undergoes maceration, tear or even total damage that leads to the loss of its biomechanical functions (Katsuragawa et al., 2010). These symptoms contribute to the abnormal joint loading, and further accelerate the degeneration of cartilage (Englund, 2008; Hunter et al., 2006; Klompmaker et al., 1992). Knowledge about the structure-mechanics relationships of meniscus ECM is thus critical for understanding joint function, documenting disease progression and designing repair strategies (Makris et al., 2011).

In the past decades, the mechanical properties of menisci in human and animals have been extensively explored via both experimental (Baro et al., 2012; Fithian et al., 1990; Proctor et al., 1989;

* Corresponding author. Tel.: +1 215 571 3821; fax: +1 215 895 4983.
E-mail address: lh535@drexel.edu (L. Han).

http://dx.doi.org/10.1016/j.jbiomech.2015.02.064
0021-9290/

Sweigart and Athanasiou, 2005) and theoretical (Spilker et al., 1992) approaches. These studies have established a knowledge base of meniscus biomechanics across species. However, biomechanical knowledge of meniscus in one critical species, mouse, is lacking. Murine models offer a unique platform to study synovial joint development and OA pathology due to its short lifespan, low cost of maintenance and availability for genetic modification (Ameye and Young, 2006; Fang and Beier, 2014). Limited by its relatively small tissue size, conventional mechanical tests are not applicable to evaluate the structure or mechanical properties of murine menisci. Without this understanding, it is challenging to study joint development or OA degradation in murine models from the perspective of meniscus biomechanics.

The objective of this study is to define the biomechanical properties of murine meniscus surface. Using atomic force microscopy (AFM)-based nanoindentation, we quantified the indentation responses of the meniscus surface from normal, male C57BL/6 mice. This study revealed the impacts of indentation rate, anatomical location and age on the mechanical properties. The indentation responses were interpreted in the context of meniscus surface collagen fibril structure quantified on 12-week old tissues. Results were compared with menisci from other species, as well as murine articular cartilage to highlight the unique properties of murine meniscus. We expect the knowledge learned from the evaluation of healthy murine meniscus to serve as a benchmark for future investigations of OA-associated mechanical symptoms of meniscus surface in various transgenic or surgery-induced murine models.

2. Methods

2.1. Sample preparation

Hind knee menisci were harvested from male C57BL/6 mice at 6, 8, 12 and 24 weeks of ages (The Jackson Laboratory, Bar Harbor, ME) via release from the meniscus-tibial tendons. Freshly dissected samples were maintained in phosphate buffered saline (PBS, pH=7.4) with protease inhibitors (Pierce Protease Inhibitor Tablets 88266, Thermo Fisher Scientific, Rockford, IL) at 4 °C for less than 24 h prior to mechanical tests. For each mouse, we tested the proximal side of both lateral and medial menisci. For the same mouse, we did not observe statistical differences in the mechanical properties of tissues from left versus right legs. We therefore tested either left or right knee menisci from one mouse, or pooled the data on the menisci of the same mouse.

Histology images were taken to show the overall morphology and location of ossification. Right knee joints from each of the 8- and 24-week old mice were harvested, decalcified, and embedded in paraffin. Serial 5-μm-thick sagittal sections were cut across the joint medial compartment. Safranin-O/FastGreen staining images showed that ossification at the anterior and posterior horns increased with age, with larger ossicles at the anterior end (Fig. 1a). This observation was consistent with previous studies (Pedersen, 1949). However, the ~50–100 μm thick central region for nanoindentation test was not ossified up to 24 weeks of age.

2.2. Atomic force microscopy (AFM)-based nanoindentation

Each meniscus was mounted on a stainless steel AFM disk via cyanoacrylate glue (Pelco Pro C300, Ted Pella, Inc.). Care was taken to ensure that the glue did not cover or infiltrate through the < 1 mm thick meniscus tissue, as later on confirmed by scanning electron microscope (SEM) images. For each meniscus, AFM-based nanoindentation was performed on the surface of the central, non-ossified region using a microspherical probe tip and a Dimension Icon AFM (BrukerNano, Santa Barbra, CA) (Fig. 1b). The spherical tip was prepared by attaching a borosilicate colloid ($R_{tip}=5.3\pm0.4$ μm, mean ± STD on $n=120$ colloids measured via optical microscope, Polysciences, Warrington, PA) onto the tipless cantilever (nominal spring constant $k\approx7.4$ N/m, AIO-TL tip C, NanoAndMore, Lady's Island, SC) using the M-Bond 610 epoxy (Polysciences) under the Dimension Icon AFM. For each meniscus, at least 10 different locations were tested up to an indentation depth of ≈0.3 μm at 10 μm/s rates. In addition, to study the rate-dependent mechanical properties of murine meniscus, for 8-week old murine menisci, indentation was repeated with 0.316–10 μm/s rates at each location. Each nanoindentation was found to result in negligible irreversible plastic deformation of the tissue, as suggested by the high repeatability of indentation curves at the same location and same indentation rate. Furthermore, to directly compare to the mechanical properties of murine articular cartilage, nanoindentation was also performed on the right hind knee medial condyle articular cartilage of 12-week old male mice at 10 μm/s indentation depth rate, following previously established procedures (Batista et al., 2014). During all the indentation measurements, meniscus and cartilage tissues were immersed in 0.15 M PBS (pH=7.4) with protease inhibitors (Pierce) to maintain the physiological-like fluid environment.

2.3. Indentation data analysis

Each indentation force versus depth, *F–D*, curve was analyzed by two methods (Fig. 1c). First, following our previous established procedure on articular cartilage (Han et al., 2011), we calculated the effective indentation modulus, E_{ind}, at each rate by fitting the entire portion of each loading *F–D* curve with Hertz model via least squares linear regression (LSLR)

$$F=\frac{4}{3}\frac{E_{ind}}{(1-\nu^2)}R_{tip}^{1/2}D^{3/2} \quad (1)$$

where R_{tip} is the tip radius (≈5 μm), and ν is the Poisson's ratio (≈0 for meniscus). The choice of Poisson's ratio was based on the estimate from tissue-level studies on other species (Sweigart et al., 2004). However, varying ν from 0–0.5 only yielded ≈25% difference in calculated E_{ind}, and did not affect the conclusions of this study.

Secondly, for each *F–D* curve, we calculated the effective indentation stiffness, S_{ind}, as the slope of the entire portion of the loading curve via LSLR

$$S_{ind}=\frac{dF}{dD}, \quad (2)$$

The coefficient of determination, R^2, was used to compare the goodness-of-fit by these two methods. For all the *F–D* curves, the tip-sample adhesion forces were found to be negligible compared to the indentation forces (~1 μN, Fig. 1c).

2.4. Scanning electron microscopy (SEM) and tapping mode AFM imaging

To qualitatively interpret the biomechanical properties of murine meniscus in the context of its matrix collagen structure, serial enzymatic digestions were carried out to enable direct visualization of collagen fibrils on the surface of 12-week old murine menisci. Immediately after nanoindentation, menisci was incubated in 0.1 mg/mL bovine pancreatic trypsin (Sigma-Aldrich, St. Louis, MO) in PBS (pH=7.4) at 37 °C for 24 h to remove proteoglycans, as previously described (Rojas et al., 2014). Tissues were then incubated in 0.4 U/mL hyaluronidase (Sigma-Aldrich) in PBS with 10 mM sodium acetate (pH=6.0) at 37 °C for 24 h to remove hyaluronan (Vanden Berg-Foels et al., 2012). After the digestion, samples were fixed with Karnovsky's fixative (Electron Microscopy Sciences, Hatfield, PA) for 3 h at room temperature, and then rinsed thoroughly with deionized water to remove chemical residuals. The samples were first dehydrated in a series of graded ethanol–water mixtures (ethanol volume ratio: 25%, 50%, 75%, 80% and 100%), each for two 10 min immersions. They were then immersed in a series of graded mixtures of hexamethyldisilazane (HMDS) (Sigma-Aldrich) and ethanol (HMDS volume ratio: 25%, 50%, 75% and 100%), each for two 10 min immersions (Bray et al., 1993). As surface tension was minimized in HMDS, the samples were dried in air overnight to retain the 3D architecture of the collagen structure and stored in a desiccator prior to imaging.

For tapping mode AFM imaging, a nanosized, pyramidal AFM tip (nominal $R_{tip}\approx10$ nm, nominal $k\approx42$ N/m, NCHV, BrukerNano) was used to visualize the meniscus surface collagen fibril architecture ($n=3$ medial menisci at 12 weeks of age) in ambient conditions using the Dimension Icon AFM. For SEM imaging, additional samples ($n=3$ medial menisci at 12 weeks of age) were thermally coated with 10 nm platinum, and imaged immediately via SEM (Supra 50vp, Zeiss, Peabody, MA). For both SEM and AFM images, the distributions of collagen diameter and alignment angle, θ, with respect to the circumferential direction were manually measured via ImageJ.

2.5. Statistical analysis

Non-parametric statistical tests were used to avoid the assumption of normal distribution. Mann-Whitney U test was performed on the average S_{ind}, or E_{ind}, of menisci from each mouse to detect whether S_{ind} or E_{ind} vary significantly between the lateral versus medial compartments, or vary between meniscus and cartilage. Kruskal-Wallis test was performed to detect the variations with respect to indentation regions (inner, middle and outer), and mouse age. Friedman test was performed to examine the rate dependence of E_{ind} or S_{ind}. To compare the linear fit versus Hertz model, Wilcoxon signed-rank test was performed on the average coefficient of determination, R^2, obtained on each mouse with both fits. Except for those presented in Fig. 2b, data obtained on one mouse were pooled, as no significant differences were found between left versus right meniscus, or between medial versus lateral compartments. In all the tests, a *p*-value of less than 0.05 was taken as statistically significant.

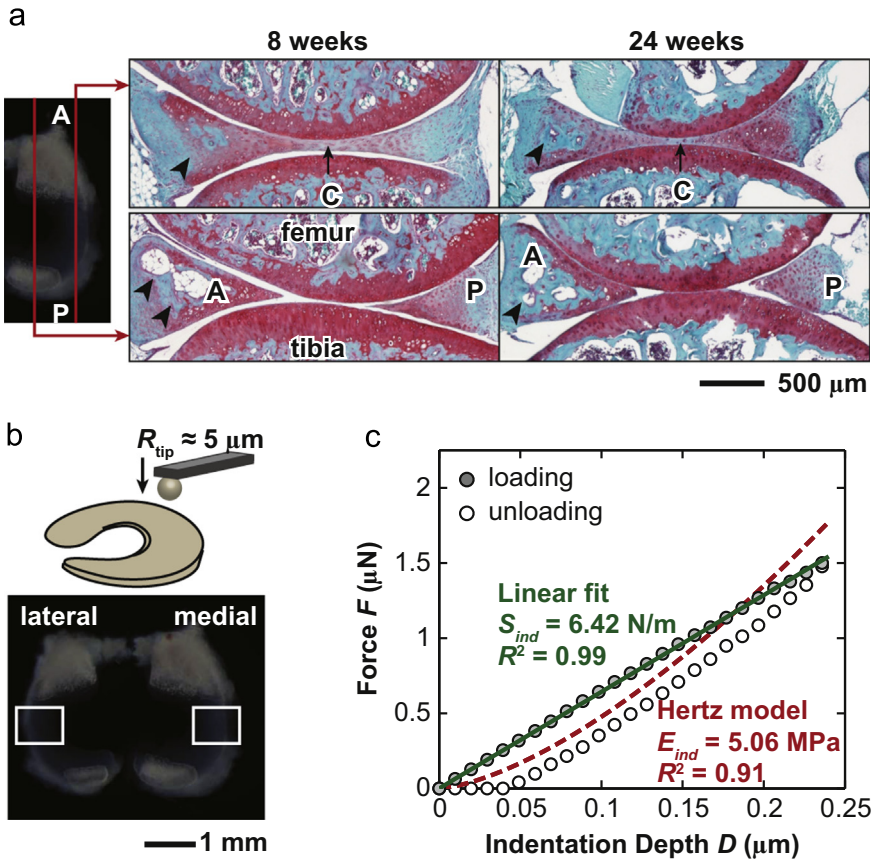

Fig. 1. AFM-based nanoindentation of murine meniscus surface. (a) Safranin-O/FastGreen histological staining of the sagittal cross-section of the medial compartments from 8- and 24-week old murine knees. Increased ossification at the anterior (A) and posterior (P) horns with age was shown as white-to-blue staining (black arrowheads). The ~ 50–100 μm thick central region (C) for nanoindentation test was not ossified. (b) Schematic of AFM-based nanoindentation on murine meniscus, where the two squares highlight the regions of interest, i.e., the proximal side, central region of each meniscus surface. (c) Typical indentation force versus depth (*F–D*) curve on one 8-week old murine medial meniscus at 10 μm/s indentation depth rate. The linear fit on the loading curve yields higher coefficient of determination, R^2, than the Hertz model. (For interpretation of the references to color in this figure legend, the reader is referred to the web version of this article.)

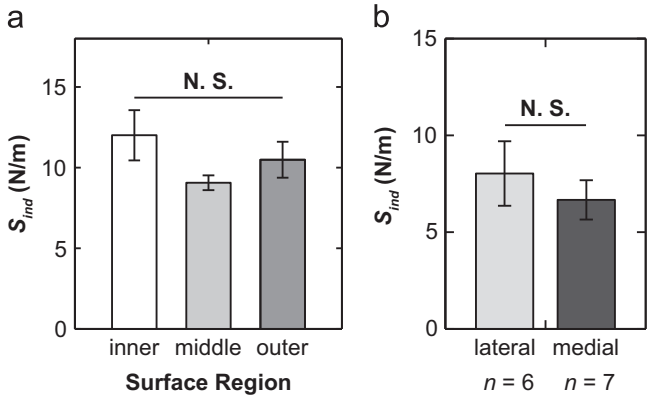

Fig. 2. Absence of mechanical heterogeneity across different anatomical sites. (a) Effective indentation stiffness, S_{ind}, showed no significant difference within the inner, middle and outer surface regions, measured on the meniscus central region of one 6-week old mouse (mean ± SEM of ≥ 8 locations in each region, $p > 0.05$ via Kruskal-Wallis test). (b) S_{ind} of lateral versus medial menisci showed no significant difference (mean ± SEM of the average S_{ind} measured on each 12-week old meniscus, $n=6$ for lateral and $n=7$ for medial menisci, $p > 0.05$ via Mann-Whitney U test). All the values were measured at 10 μm/s indentation depth rate.

3. Results

For all menisci, most indents yielded a unique, non-Hertzian indentation response. The *F–D* curves were found to behave more linearly at all tested rates, rather than the typical $F–D^{3/2}$ Hertzian pattern (Fig. 1c). For each *F–D* curve, S_{ind} was calculated to provide a more precise description of the *F–D* dependence. The Hertz model-based E_{ind} was also calculated to enable direct comparison with the moduli of menisci in other species, and with those of murine articular cartilage.

We did not find significant heterogeneity across different anatomical locations. On the proximal side of each meniscus, S_{ind} was found not to vary significantly across the inner, middle and outer regions (Fig. 2a). We therefore pooled the data obtained at all three regions from each meniscus. In addition, absence of significance in S_{ind} was found between the lateral and medial menisci (Fig. 2b). Similar to other soft tissues, significant rate dependence was detected here, where increasing indentation rate from 0.316 to 10 μm/s significantly increased S_{ind}. Furthermore, the linear *F–D* behaviors were persistent at all the tested rates (Fig. 3).

Within the tested murine age from 6 to 24 weeks, we did not find significant trend in S_{ind} (or E_{ind}). S_{ind} was found to be 9.6 ± 1.0 N/m, 7.8 ± 1.0 N/m, 7.3 ± 0.9 N/m and 7.5 ± 1.0 N/m at 6, 8, 12 and 24 weeks of age, respectively (Fig. 4a). When the Hertz model was applied, E_{ind} was 9.2 ± 1.6 MPa, 6.7 ± 1.1 MPa, 6.1 ± 0.8 MPa and 7.0 ± 1.2 MPa, at 6, 8, 12 and 24 weeks of age, respectively (Fig. 4b). In all tested ages, the coefficient of determination in LSLR, R^2, was significantly higher when using the linear fit than using the Hertz model (Fig. 4c). When compared to its direct contact counterpart, the articular cartilage surface, the murine meniscus surface appeared much stiffer. As shown in Fig. 5, nanoindentation on 12-week old murine cartilage yielded E_{ind} of 1.4 ± 0.1 MPa, ≈ 4 × lower than the moduli of meniscus at the same age.

Results from tapping mode AFM and SEM imaging on 12-week old meniscus surfaces were consistent ($p > 0.05$ via Mann-Whitney test), and were therefore pooled for analysis. The images yielded unique structural features of murine meniscus surface. Unlike the human tissues, we found the majority of surface collagen fibrils are aligned nearly along the circumferential direction as fibril bundles (Fig. 6a–c). The diameters of collagen fibrils were found to be 49.8 ± 9.5 nm (mean $\pm$ STD of 325 fibrils on the medial menisci of six 12-week old mice, 232 from SEM and 93 from AFM, Fig. 6d), similar to those of C57BL/6 wild-type murine articular cartilage surface (Batista et al., 2014). In addition, the absolute values of the angle of each fibril alignment with respect to the circumferential direction, θ, were found to be $21.9 \pm 20.7^\circ$ (429 fibrils on six 12-week old mice, 324 from SEM and 105 from AFM, Fig. 6e). The median of θ was 15.0°. As shown by the distribution of θ, in addition the dominance of circumferentially aligned fibril bundles, there also existed transversely aligned fibrils interdigitating throughout these circumferential fibril bundles (e.g., white arrowheads in Fig. 6b and c), with a marginal preferential alignment along the radial direction (e.g., 3.7 $\pm$ 0.9% of fibrils at $70^\circ \le \theta < 80^\circ$, Fig. 6e).

4. Discussion

4.1. Non-Hertzian indentation responses of murine meniscus surface

The linear *F–D* indentation response of murine meniscus surface is reported here for the first time (Figs. 1c, 3 and 5). This non-Hertzian behavior likely originates from the densely packed, highly anisotropic collagen fibril structure of the meniscus surface (Fig. 6). As revealed by SEM and AFM imaging on the 12-week old menisci, the surface is dominated by densely packed, circumferentially aligned fibril bundles, interdigitated by sparsely distributed, transversely aligned fibrils (white arrowheads in Fig. 6b and c). This structure leads to substantial tension–compression asymmetry. When nanoindentation was performed normal to the surface, forces could mainly originate from the fibril tension resistance. In such highly aligned, densely packed fibril bundles, when fibril stretching, rather than uncrimping/realignment, dominates its deformation, stresses can travel along the fibrils much further beyond the local contact region (Wang et al., 2014). In this experiment, stresses likely transmit along the fibril bundles to a distance orders of magnitude ($\gg$10 μm) greater than the tip-sample contact radius ($\approx$2.2 μm at 0.5 μm indentation depth). As a result, stresses were not localized, and indentation forces may not directly scale with the tip-sample contact area, as would be predicted by the Hertz model.

Another possible origin of this non-Hertzian response is the time-dependent poroviscoelasticity. It has been shown that when the indentation time is comparable with the characteristic viscoelasticity time ($t_{indent}/\tau_{visco} \sim 1$), *F–D* curves measured by a spherical tip follows a linear pattern (Sakai, 2002). However, we observed the linear *F–D* curves at all indentation rates (0.316–10 μm/s, Fig. 3a), rather than at one particular rate. While the rate dependent indentation behavior was only reported for 8-week old menisci (Fig. 3), this linear *F–D* relationship was found to persist at other ages (6–24 weeks) in the range of 0.1–10 μm/s indentation rates as well (data not shown). Thus, it is less likely

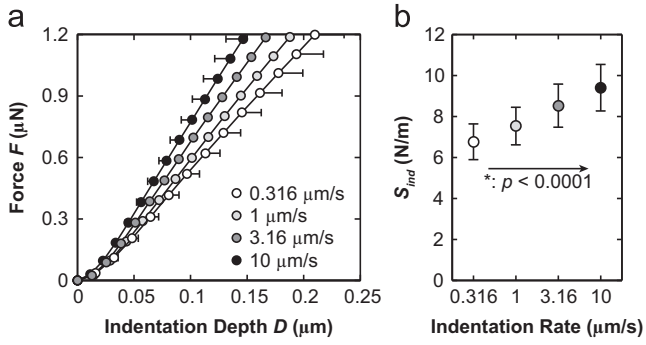

Fig. 3. Indentation rate-dependent mechanical properties of murine meniscus surface. (a) Indentation force versus depth curves at 0.316–10 μm/s indentation depth rates. (b) Significant rate dependence of S_{ind} was detected via Friedman's test ($p < 0.0001$). For both panels, data shown are mean $\pm$ SEM of $\ge$ 8 locations on one 8-week old medial meniscus.

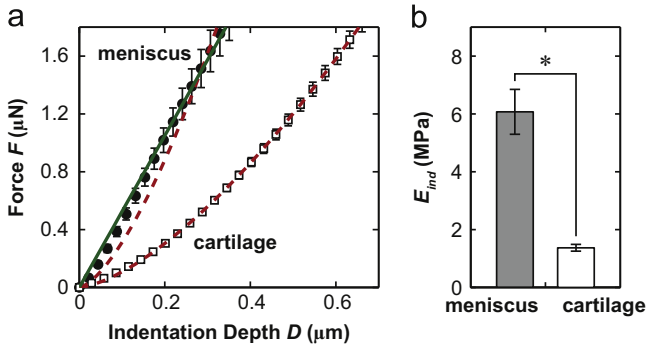

Fig. 5. Comparison of the mechanical properties between murine meniscus and cartilage surfaces. (a) Typical indentation *F–D* curves on the one medial meniscus and medial condyle cartilage (mean $\pm$ SEM of $\ge$ 10 positions each, 12 weeks age). The green solid line is the linear fit for meniscus data, and red dashed lines are Hertzian fits for both. (b) Meniscus surfaces ($n=13$) showed significantly higher E_{ind} than articular cartilage surfaces ($n=6$) at 12 weeks age (*: $p < 0.0001$ via Mann-Whitney U test). All the data were measured at 10 μm/s indentation depth rate. (For interpretation of the references to color in this figure legend, the reader is referred to the web version of this article.)

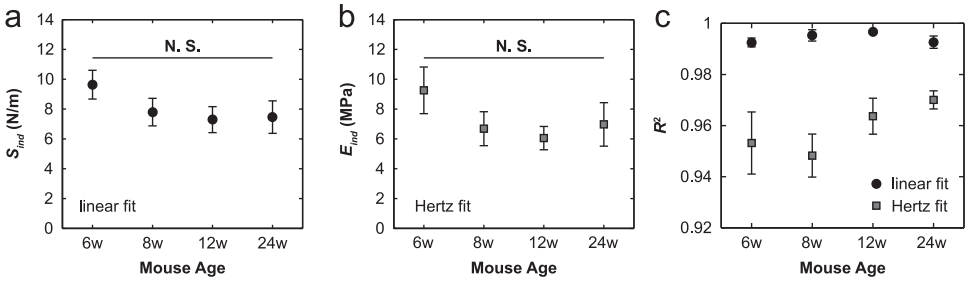

Fig. 4. Mechanical properties of murine meniscus surface at different ages. (a, b) Effective indentation stiffness, S_{ind} (a), and modulus, E_{ind} (b), of the proximal side meniscus surface at 6 weeks ($n=5$), 8 weeks ($n=10$), 12 weeks ($n=13$) and 24 weeks ($n=5$) of ages showed no significant age dependence ($p > 0.05$ via Kruskal-Wallis test). (c) Comparison of coefficient of determination, R^2, calculated via the fits of S_{ind} and E_{ind}. The linear fit yields significantly higher R^2 than the Hertz model ($p < 0.0001$ via Wilcoxon signed rank test). For all three panels, data shown are mean $\pm$ SEM of the average values measured on meniscus at the given age cohort at 10 μm/s indentation depth rate.

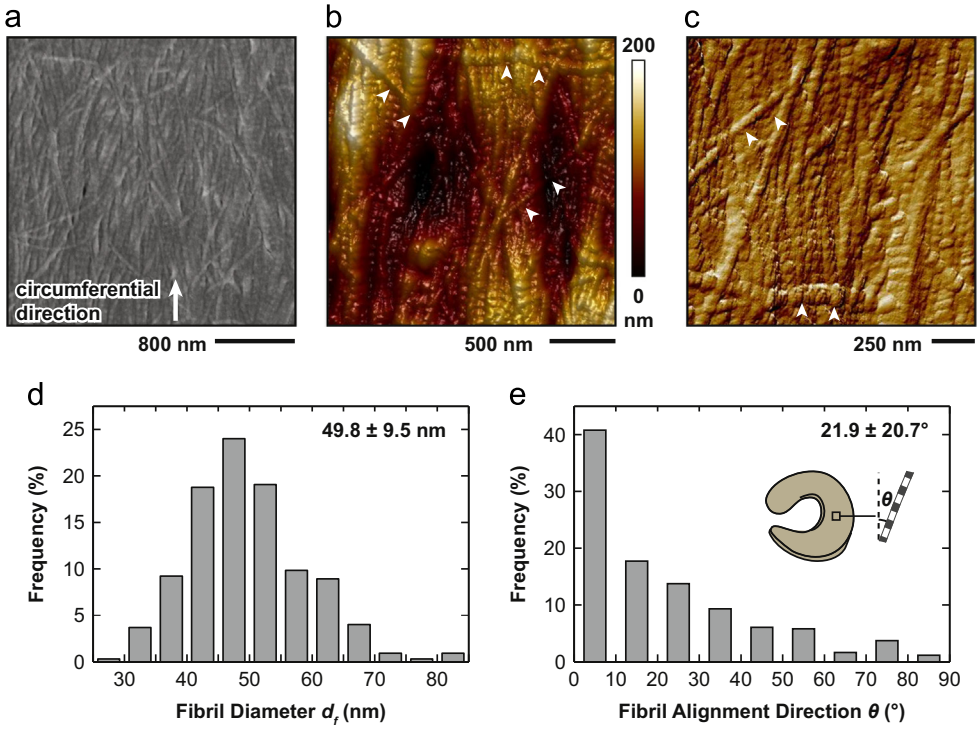

Fig. 6. Collagen architecture of murine meniscus surface. Typical (a) SEM and tapping mode AFM (b) height and (c) amplitude images at different scales show that collagen fibrils are mostly aligned as bundles along the circumferential direction on meniscus surface, interdigitated by transversely aligned fibrils (white arrowheads in b). (d, e) Histograms of (d) collagen diameter and (e) collagen alignment with respect to the circumferential direction, respectively. Values reported are mean ± STD of 325 fibrils for diameter (232 from SEM, 93 from AFM), and 429 fibrils for alignment direction (324 from SEM, 105 from AFM) from six 12-week old medial menisci.

that poroviscoelasticity is the dominating factor. We hypothesize that the tension resistance of meniscus surface collagen fibrils is the main factor of this non-Hertzian *F–D* response, while poroviscoelastic time-dependence may play a minor role. Current studies are aimed at quantitatively investigating the origins of this non-Hertzian response by combining AFM imaging, AFM-nanoindentation at different length scales and fibril-reinforce finite element models (Soulhat et al., 1999) to quantitatively reveal the nanostructure-nanomechanics relationships of murine meniscus and the associated age-dependence.

4.2. Absence of anatomical location dependence

We did not observe significant variations in S_{ind} (or E_{ind}) across the inner to outer regions on each meniscus (Fig. 2a), or between the lateral versus medial menisci (Fig. 2b). This lack of mechanical heterogeneity may be associated with the unique biomechanical functions of the meniscus surface. These functions include load distribution and transmission with cartilage, and the maintenance of meniscus tissue structural integrity (Andriacchi et al., 2004; Walker and Erkman, 1975). A structurally more homogeneous surface layer could be more effective in distributing stress to the interior and may reduce the risk of meniscus tear. This phenomenon of homogeneity is consistent with previous studies on the instantaneous modulus of skeletally mature porcine meniscus measured by AFM-nanoindentation (Sanchez-Adams et al., 2013), and local tissue strain distribution of young bovine menisci via depth-dependent strain monitoring (Lai and Levenston, 2010). Interestingly, this relative homogeneity of the surface is in high contrast to the salient heterogeneity of the interior meniscus. Different regions in the meniscus interior are known to have distinctive mechanical functions. As shown previously for porcine menisci, the outer (red) zone that mainly sustains circumferential tensile stresses is mechanically distinct from the inner (white) zone (Sanchez-Adams et al., 2013) that mostly undergoes compression (Makris et al., 2011).

4.3. Absence of age-dependence

We also did not observe significant age-dependence in S_{ind} or E_{ind} from young, immature (6 weeks) to mature (24 weeks) mice (Fig. 4). This lack of age-dependence could be attributed to the dominance of type I collagen-based fibrils and negligible concentration of proteoglycan content on meniscus surface (Moyer et al., 2013), as the turnover of collagen is known to be markedly longer than other matrix constituents. For example, in human femoral head cartilage, the metabolic half-life of type II-dominated collagen is ≈117 years (Verzijl et al., 2000), while that of aggrecan is ≈3.4 years (Maroudas et al., 1998). In human skin, the half-life of type I-dominated collagen is ≈15 years (Verzijl et al., 2000). The half-life of murine meniscus collagen has not been quantified. However, it is reasonable to expect a collagen network half-life comparable to the life expectancy of mice, or at least, to the age span (6 to 24 weeks) of this study. It is therefore likely that meniscus structure and mechanics exhibit much less age-dependent variations within the tested age than the aggrecan-rich cartilage. Interestingly, while we did not find significant age dependence in meniscus (Fig. 4), the density and modulus of cortical bone from the same C57BL/6 mouse strain was found to significantly increase with age within 4 to 24 weeks of age. However, this increase in modulus was marginal after 8 weeks of age, and was highly correlated with increase in the degree of mineralization (Somerville et al., 2004). For the central region of meniscus, in the absence of mineralization, the temporal trend of development and maturation could be different from that of cortical bone. We believe that future studies targeted to younger and older mice can further elucidate the mechanical implications of meniscus, as well as its association with skeletal development and aging.

4.4. Comparison to meniscus of other species

Interestingly, the murine meniscus surface showed significantly higher E_{ind} than those of other species measured via nano- to microindentations. In this study, E_{ind} of 12-week old menisci was 6.1 ± 0.8 MPa (Fig. 3b). In comparison, for skeletally mature porcine meniscus surface, AFM-based nanoindentation with an $R_{tip} \approx 2.5$ μm spherical tip showed moduli in the range of 36 ± 7 kPa (reported as mean $\pm$ SD, outer zone) to 60 ± 15 kPa (inner zone) (Sanchez-Adams et al., 2013). For human meniscus surface, instrumented microindentation with an $R_{tip} \approx 150$ μm spherical tip showed steady state modulus of 1.65 ± 0.13 MPa for 57–70 years old tissues (Moyer et al., 2012). This markedly higher E_{ind} of murine meniscus is likely associated with their smaller body weight than other species. Recently, a negative allometric scaling was found between articular cartilage thickness and body mass across many species, including mouse, human and others. This relation was hypothesized to contribute to a decrease in cartilage biomechanical properties as increasing body weight (Malda et al., 2013). This hypothesis was supported by our previous nanoindentation work on wild-type murine knee cartilage, where murine cartilage was found to be significantly stiffer ($E_{ind} \sim 1$ MPa) (Batista et al., 2014) than cartilage of larger species, including porcine (McLeod et al., 2013), bovine (Nia et al., 2011) and human (Stolz et al., 2009) tissues ($E_{ind} \sim 0.1$ MPa). For meniscus, there has been no systematic study on the relationship between body mass and tissue size across species. However, since the thickness of meniscus is similar to articular cartilage in both mouse ($\sim$50–100 μm in the central region, Fig. 1a) and human ($\sim$2 mm; Wenger et al., 2013), it is likely that similar allometric scaling law is also present. As supported by recent tissue-level studies (Joshi et al., 1995; Sweigart et al., 2004), macroindentation measurements found that the smaller lapine menisci had significantly higher aggregate moduli than the larger human, porcine and bovine tissues (Sweigart et al., 2004).

4.5. Comparison to murine articular cartilage

The moduli of murine meniscus surface were significantly higher than its direct contact counterpart, the articular cartilage ($E_{ind} = 1.4 \pm 0.1$ MPa, Fig. 5b). In addition, as shown in this and previous (Batista et al., 2014) studies, indentation of articular cartilage resulted in typical Hertzian-like *F–D* curves (Fig. 5a). The surface layer of articular cartilage is mostly composed of transversely aligned, type II-dominated collagen fibrils, with higher proteoglycan concentrations than meniscus (Xia et al., 2008). The lower cartilage moduli are likely associated with the less organized, less densely packed, or less pre-stretched collagen fibril networks on the surface. In comparison to meniscus, the presence of abundant proteoglycans in articular cartilage may also contribute to the stress localization and higher degree of isotropy, and thus, lead to more Hertzian-like indentation responses.

4.6. Implications for murine model-based osteoarthritis studies

Mechanical knowledge obtained in this study can be applied to murine-based osteoarthritis studies. Recently, AFM-based nanomechanical tests on murine cartilage have become a valuable tool for investigating the articular cartilage biomechanical function and pathogenesis of OA (Batista et al., 2014; Nia et al., 2015; Stolz et al., 2009; Willard et al., 2014). Successful execution of AFM-based nanoindentation on murine cartilage demonstrated the potential of using similar approaches to provide valuable insights into the roles of meniscus in the development of OA. While OA is now recognized as a whole-joint disease (Poole, 2012), understanding of the function of meniscus and its interaction with articular cartilage during OA progression is very limited. A biomechanical focus on murine meniscus can thus provide a novel platform for investigating individual mechanical changes of joint tissues that occur and result in OA. For example, it is suggested that in articular cartilage, OA initiates from superficial layer before propagating to the interior (Saarakkala et al., 2010), while the propagation pattern of OA in meniscus is unclear (Pauli et al., 2011). Based on the knowledge of healthy, normal mice, future studies on the concomitant mechanical changes at the meniscus–cartilage contact interfaces may be used as a novel biomarker for the detection and evaluation of OA when combined with clinically relevant OA models, such as the destabilization of the medial meniscus surgery (Glasson et al., 2007).

5. Conclusions

In this study, we quantified the nanomechanical properties of murine meniscus surface via AFM-based nanoindentation. A non-Hertzian, linear *F–D* indentation response was detected on normal, healthy murine meniscus surface at 6–24 weeks age. This behavior is likely associated with the highly anisotropic, circumferential collagen fibril bundle-dominated architecture. The indentation modulus/stiffness showed negligible dependence on tested anatomical locations or mouse age. In addition, murine menisci were found to be $\approx 4\times$ stiffer than murine articular cartilage. To our knowledge, this is the first study that focused on the mechanical properties of murine meniscus. It is hoped that the knowledge obtained here can lay the ground for future explorations of meniscus developmental biology and OA pathology using transgenic or surgery-induced OA models.

Conflict of interest statement

The authors of this study have no personal or financial conflicts of interest with this work. All authors were fully involved in the study and preparation of this manuscript and the material within has not been and will not be submitted for publication elsewhere.

Acknowledgments

This work was supported by the Faculty Start-up Grant at Drexel University (LH), the National Institutes of Health (Grants AR063905 to VR, AR060991 to LQ and AR033236 to CO and AJG). We also thank Dr. R. L. Mauck, Dr. L. J. Soslowsky and Dr. V. B. Shenoy for valuable discussions.

References

Ameye, L.G., Young, M.F., 2006. Animal models of osteoarthritis: lessons learned while seeking the 'Holy Grail'. Curr. Opin. Rheumatol. 18, 537–547.
Andriacchi, T.P., Mündermann, A., Smith, R.L., Alexander, E.J., Dyrby, C.O., Koo, S., 2004. A framework for the in vivo pathomechanics of osteoarthritis at the knee. Ann. Biomed. Eng. 32, 447–457.
Aspden, R.M., Yarker, Y.E., Hukins, D.W.L., 1985. Collagen orientations in the meniscus of the knee joint. J. Anat. 140, 371–380.
Baro, V.J., Bonnevie, E.D., Lai, X., Price, C., Burris, D.L., Wang, L., 2012. Functional characterization of normal and degraded bovine meniscus: rate-dependent indentation and friction studies. Bone 51, 232–240.
Batista, M.A., Nia, H.T., Önnerfjord, P., Cox, K.A., Ortiz, C., Grodzinsky, A.J., Heinegård, D., Han, L., 2014. Nanomechanical phenotype of chondroadherin-null murine articular cartilage. Matrix Biol. 38, 84–90.
Bray, D.F., Bagu, J., Koegler, P., 1993. Comparison of hexamethyldisilazane (HMDS), peldri II, and critical-point drying methods for scanning electron-microscopy of biological specimens. Microsc. Res. Tech. 26, 489–495.
Englund, M., 2008. The role of the meniscus in osteoarthritis genesis. Rheum. Dis. Clin. North Am. 34, 573–579.
Fang, H., Beier, F., 2014. Mouse models of osteoarthritis: modelling risk factors and assessing outcomes. Nat. Rev. Rheumatol. 10, 413–421.

Fithian, D.C., Kelly, M.A., Mow, V.C., 1990. Material properties and structure-function-relationships in the menisci. Clin. Orthop. Relat. Res. 252, 19–31.
Glasson, S.S., Blanchet, T.J., Morris, E.A., 2007. The surgical destabilization of the medial meniscus (DMM) model of osteoarthritis in the 129/SvEv mouse. Osteoarthr. Cartil. 15, 1061–1069.
Han, L., Frank, E.H., Greene, J.J., Lee, H.-Y., Hung, H.-H.K., Grodzinsky, A.J., Ortiz, C., 2011. Time-dependent nanomechanics of cartilage. Biophys. J. 100, 1846–1854.
Herwig, J., Egner, E., Buddecke, E., 1984. Chemical changes of human knee joint menisci in various stages of degeneration. Ann. Rheum. Dis. 43, 635–640.
Hunter, D.J., Zhang, Y.Q., Niu, J.B., Tu, X., Amin, S., Clancy, M., Guermazi, A., Grigorian, M., Gale, D., Felson, D.T., 2006. The association of meniscal pathologic changes with cartilage loss in symptomatic knee ostoearthritis. Arthritis Rheum. 54, 795–801.
Joshi, M.D., Suh, J.-K., Marui, T., Woo, S.L.-Y., 1995. Interspecies variation of compressive biomechanical properties of the meniscus. J. Biomed. Mater. Res. 29, 823–828.
Katsuragawa, Y., Saitoh, K., Tanaka, N., Wake, M., Ikeda, Y., Furukawa, H., Tohma, S., Sawabe, M., Ishiyama, M., Yagishita, S., Suzuki, R., Mitomi, H., Fukui, N., 2010. Changes of human menisci in osteoarthritic knee joints. Osteoarthr. Cartil. 18, 1133–1143.
Klompmaker, J., Jansen, H.W.B., Veth, R.P.H., Nielsen, H.K.L., de Groot, J.H., Pennings, A.J., Kuijer, R., 1992. Meniscal repair by fibrocartilage? An experimental study in the dog. J. Orthop. Res. 10, 359–370.
Lai, J.H., Levenston, M.E., 2010. Meniscus and cartilage exhibit distinct intra-tissue strain distributions under unconfined compression. Osteoarthr. Cartil. 18, 1291–1299.
Makris, E.A., Hadidi, P., Athanasiou, K.A., 2011. The knee meniscus: structure-function, pathophysiology, current repair techniques, and prospects for regeneration. Biomaterials 32, 7411–7431.
Malda, J., de Grauw, J.C., Benders, K.E.M., Kik, M.J.L., van de Lest, C.H.A., Creemers, L.B., Dhert, W.J.A., van Weeren, P.R., 2013. Of mice, men and elephants: the relation between articular cartilage thickness and body mass. PLoS One 8, e57683.
Maroudas, A., Bayliss, M.T., Uchitel-Kaushansky, N., Schneiderman, R., Gilav, E., 1998. Aggrecan turnover in human articular cartilage: use of aspartic acid racemization as a marker of molecular age. Arch. Biochem. Biophys. 350, 61–71.
McLeod, M.A., Wilusz, R.E., Guilak, F., 2013. Depth-dependent anisotropy of the micromechanical properties of the extracellular and pericellular matrices of articular cartilage evaluated via atomic force microscopy. J. Biomech. 46, 586–592.
Moyer, J.T., Abraham, A.C., Donahue, T.L.H., 2012. Nanoindentation of human meniscal surfaces. J. Biomech. 45, 2230–2235.
Moyer, J.T., Priest, R., Bouman, T., Abraham, A.C., Donahue, T.L.H., 2013. Indentation properties and glycosaminoglycan content of human menisci in the deep zone. Acta Biomater. 9, 6624–6629.
Nia, H.T., Gauci, S., Azadi, M., Hung, H.-H., Frank, E., Fosang, A.J., Ortiz, C., Grodzinsky, A.J., 2015. High-bandwidth AFM-based rheology is a sensitive indicator of early cartilage aggrecan degradation relevant to mouse models of osteoarthritis.
J. Biomech. 48, 162–165.
Nia, H.T., Han, L., Li, Y., Ortiz, C., Grodzinsky, A.J., 2011. Poroelasticity of cartilage at the nanoscale. Biophys. J. 101, 2304–2313.
Pauli, C., Grogan, S.P., Patil, S., Otsuki, S., Hasegawa, A., Koziol, J., Lotz, M.K., D'Lima, D.D., 2011. Macroscopic and histopathologic analysis of human knee menisci in aging and osteoarthritis. Osteoarthr. Cartil. 19, 1132–1141.
Pedersen, H.E., 1949. The ossicles of the semilunar cartilages of rodents. Anat. Rec. 105, 1–9.
Petersen, W., Tillmann, B., 1998. Collagenous fibril texture of the human knee joint menisci. Anat. Embryol. 197, 317–324.
Poole, A.R., 2012. Osteoarthritis as a whole joint disease. HSSJ 8, 4–6.
Proctor, C.S., Schmidt, M.B., Whipple, R.R., Kelly, M.A., Mow, V.C., 1989. Material properties of the normal medial bovine meniscus. J. Orthop. Res. 7, 771–782.
Rojas, F.P., Batista, M.A., Lindburg, C.A., Dean, D., Grodzinsky, A.J., Ortiz, C., Han, L., 2014. Molecular adhesion between cartilage extracellular matrix macromolecules. Biomacromolecules 15, 772–780.
Saarakkala, S., Julkunen, P., Kiviranta, P., Mäkitalo, J., Jurvelin, J.S., Korhonen, R.K., 2010. Depth-wise progression of osteoarthritis in human articular cartilage: investigation of composition, structure and biomechanics. Osteoarthr. Cartil. 18, 73–81.
Sakai, M., 2002. Time-dependent viscoelastic relation between load and penetration for an axisymmetric indenter. Philos. Mag. A 82, 1841–1849.
Sanchez-Adams, J., Wilusz, R.E., Guilak, F., 2013. Atomic force microscopy reveals regional variations in the micromechanical properties of the pericellular and extracellular matrices of the meniscus. J. Orthop. Res. 31, 1218–1225.
Skaggs, D.L., Warden, W.H., Mow, V.C., 1994. Radial tie fibers influence the tensile properties of the bovine medial meniscus. J. Orthop. Res. 12, 176–185.
Somerville, J.M., Aspden, R.M., Armour, K.E., Armour, K.J., Reid, D.M., 2004. Growth of C57BL/6 mice and the material and mechanical properties of cortical bone from the tibia. Calcif. Tissue Int. 74, 469–475.
Soulhat, J., Buschmann, M.D., Shirazi-Adl, A., 1999. A fibril-network-reinforced biphasic model of cartilage in unconfined compression. J. Biomech. Eng. 121, 340–347.
Spilker, R.L., Donzelli, P.S., Mow, V.C., 1992. A transversely isotropic biphasic finite element model of the meniscus. J. Biomech. 25, 1027–1045.
Stolz, M., Gottardi, R., Raiteri, R., Miot, S., Martin, I., Imer, R., Staufer, U., Raducanu, A., Düggelin, M., Baschong, W., Daniels, A.U., Friederich, N.F., Aszodi, A., Aebi, U., 2009. Early detection of aging cartilage and osteoarthritis in mice and patient samples using atomic force microscopy. Nat. Nanotechnol. 4, 186–192.
Sweigart, M.A., Athanasiou, K.A., 2005. Tensile and compressive properties of the medial rabbit meniscus. Proc. Inst. Mech. Eng. H 219, 337–347.
Sweigart, M.A., Zhu, C.F., Burt, D.M., deHoll, P.D., Agrawal, C.M., Clanton, T.O., Athanasiou, K.A., 2004. Intraspecies and interspecies comparison of the compressive properties of the medial meniscus. Ann. Biomed. Eng. 32, 1569–1579.
Vanden Berg-Foels, W.S., Scipioni, L., Huynh, C., Wen, X., 2012. Helium ion microscopy for high-resolution visualization of the articular cartilage collagen network. J. Microsc. 246, 168–176.
Verzijl, N., DeGroot, J., Thorpe, S.R., Bank, R.A., Shaw, J.N., Lyons, T.J., Bijlsma, J.W.J., Lafeber, F.P.J.G., Baynes, J.W., TeKoppele, J.M., 2000. Effect of collagen turnover on the accumulation of advanced glycation end products. J. Biol. Chem. 275, 39027–39031.
Voloshin, A.S., Wosk, J., 1983. Shock absorption of meniscectomized and painful knees: a comparative in vivo study. J. Biomed. Eng. 5, 157–161.
Walker, P.S., Erkman, M.J., 1975. The role of the menisci in force transmission across the knee. Clin. Orthop. Relat. Res., 184–192.
Wang, H., Abhilash, A.S., Chen, C.S., Wells, R.G., Shenoy, V.B., 2014. Long range force transmission in fibrous matrices enabled by tension-driven alignment of fibers. Biophys. J. 107, 2592–2603.
Wenger, A., Wirth, W., Hudelmaier, M., Noebauer-Huhmann, I., Trattnig, S., Bloecker, K., Frobell, R.B., Kwoh, C.K., Eckstein, F., Englund, M., 2013. Meniscus body position, size, and shape in persons with and persons without radiographic knee osteoarthritis: quantitative analyses of knee magnetic resonance images from the osteoarthritis initiative. Arthritis Rheum. 65, 1804–1811.
Willard, V.P., Diekman, B.O., Sanchez-Adams, J., Christoforou, N., Leong, K.W., Guilak, F., 2014. Use of cartilage derived from murine induced pluripotent stem cells for osteoarthritis drug screening. Arthritis Rheumatol. 66, 3062–3072.
Xia, Y., Zheng, S., Bidthanapally, A., 2008. Depth-dependent profiles of glycosaminoglycans in articular cartilage by μMRI and histochemistry. J. Magn. Reson. Imaging 28, 151–157.

Harvard Medical School/Harvard School of Dental Medicine

Date Prepared: 09/24/2015

Name: RUIRUI SHI

Office Address: Harvard School of Dental Medicine, Developmental Biology, REB 513, 188 Longwood Ave, Boston, MA 02115

Work Phone: 617-432-5912

Work Email: RUIRUI_SHI@HSDM.HARVARD.EDU

Work FAX: 617-432-3246

Education

2008	BA	Stomatology	Weifang Medical University
2013	MD, PhD	Oral Pathology (Tie-Jun Li)	Peking University School of Stomatology

Postdoctoral Training

08/13-02/15	Research Fellow	Morphology (Tie-Jun Li)	Peking University School and Hospital of Stomatology
02/15-	Research Fellow	Developmental Biology (Vicki Rosen)	Harvard School of Dental Medicine

Faculty Academic Appointments

08/13-	Research Associate	The Central Laboratory	Peking University School and Hospital of Stomatology

Appointments at Hospitals/Affiliated Institutions

08/13-	Research Associate	The Central Laboratory Morphological Division	Peking University School and Hospital of Stomatology

Honors and Prizes

2013	The First-Class Prize of Wrigley's Extra Scholarships	Chinese Stomatological Association	Research

2013	Excellent Doctoral Dissertation	Peking University	Research

Report of Funded and Unfunded Projects

Funding Information

Current

2013-2015 The role of Gli2 in the pathogenesis of fibrous dysplasia
Career development/YS0203
PI($1,700)
The major goal of the study is to evaluate the impact of Gli2 on the osteogenesis impairment of fibrous dsyplasia.

Report of Local Teaching and Training

Teaching of Students in Courses

2010	Oral Histopathology 3rd year and 4th year dental students	Peking University School of Stomatology 2-hr sessions per wk for 12wks

Report of Scholarship

Publications

Peer reviewed publications in print or other media

Rui-Rui Shi, Xue-Fen Li, Ran Zhang, Yan Chen, Tie-Jun Li. GNAS mutational analysis in differentiating fibrous dysplasia and ossifying fibroma of the jaw. Modern Pathology 2013; 26:1023-31.